Materials Science & Engineering A 925 (2025) 147904

Contents lists available at ScienceDirect

Materials Science & Engineering A

journal homepage: www.elsevier.com/locate/msea

Engineering the deformation-induced martensitic transformation in a medium Mn steel containing core-shell austenite particles

Shichun Liu [a], Jun Chai [a,*], Xinhao Wan [a,**], Yan Wang [a], Zhigang Yang [a], Sybrand van der Zwaag [a,b], Hao Chen [a]

[a] Key Laboratory of Advanced Materials of Ministry of Education, School of Materials Science and Engineering, Tsinghua University, Beijing, China
[b] Faculty of Aerospace Engineering, Technische Universiteit Delft, Delft, the Netherlands

ARTICLE INFO

Keywords:
Chemically heterogeneous
Mechanical stability
Retained austenite
Deformation induced martensite transformation
Chemical boundary engineering

ABSTRACT

This work further investigated the mechanical properties of chemically heterogeneous core-shell austenite. It demonstrated the ability to enhance work hardening capacity and mitigate the formation of the Lüders band. Both experiments and molecular dynamics simulations confirmed that the Mn chemical boundary acts as a barrier to martensitic transformation during deformation.

1. Introduction

Medium Mn steels (MMS) are part of the third generation of advanced high-strength steels (AHSSs) and have attracted significant attention due to their impressive combination of strength and ductility [1–3]. It is widely acknowledged that the mechanical performance of MMS is influenced not only by the properties of the ferritic/bainitic/martensitic matrix, but also by the presence of metastable retained austenite (RA) [4–8]. The transformation of the soft metastable RA into the hard martensite phase enhances work hardening capacity through the transformation-induced plasticity (TRIP) effect [9,10]. A good understanding of deformation-induced martensitic transformation (DIMT) and the parameters controlling it is crucial for the further development of MMS. The transformation of metastable austenite during deformation is governed by multiple factors, including stress state, chemical composition, strain rate, and grain size, all of which play pivotal roles in determining the kinetics and mechanics of this phase transformation [11,12].

RA in MMS is typically obtained through an austenite reversion treatment (ART), which leading to the formation of a structure that includes ferrite and austenite, resulting in Mn and C partitioning from ferrite into the austenite [13,14]. Generally, the reverted austenite grains produced via the traditional ART process are chemically homogeneous in Mn and C [15]. In contrast, retained austenite grains with chemically heterogeneous C and/or Mn distributions have shown a great potential to enhance the mechanical properties [16–19]. The present authors developed a compositional core-shell structured austenite in cold-rolled MMS with a low Mn content in the core and a high Mn content in the shell, through a process known as Flash-ART [20]. The low Mn core forms during rapid heating to the flash peak temperature, while the Mn-enriched shell develops during the subsequent isothermal hold at the ART temperature. This innovative processing route results in a much higher amount of RA, with sufficient thermal and broader mechanical stability range compared to the conventional ART process. Similarly, Sun et al. [21] devised a strategy for producing RA with a gradient in Mn concentration, which results in a spectrum of mechanical stability. This gradient has been shown to prolong the TRIP effect. Accidently, Zhang et al. [22] discovered that the presence of austenite with a core-shell structure through two-step ART process significantly enhances the resistance to hydrogen embrittlement in MMS. It has been proposed that the sequential transformation of austenite, with the core transforming first, prevents the formation and expansion of hydrogen-induced cracks at the boundaries connecting ferrite and deformation-induced martensite. Thus, a well-engineered chemical heterogeneity in austenite appears capable of overcoming the limitations of the conventional ART process, further improving both

* Corresponding author.
** Corresponding author.
E-mail addresses: stormchai@gmail.com (J. Chai), wuxinzhichang@163.com (X. Wan).

https://doi.org/10.1016/j.msea.2025.147904
Received 12 November 2024; Received in revised form 25 December 2024; Accepted 20 January 2025
Available online 27 January 2025

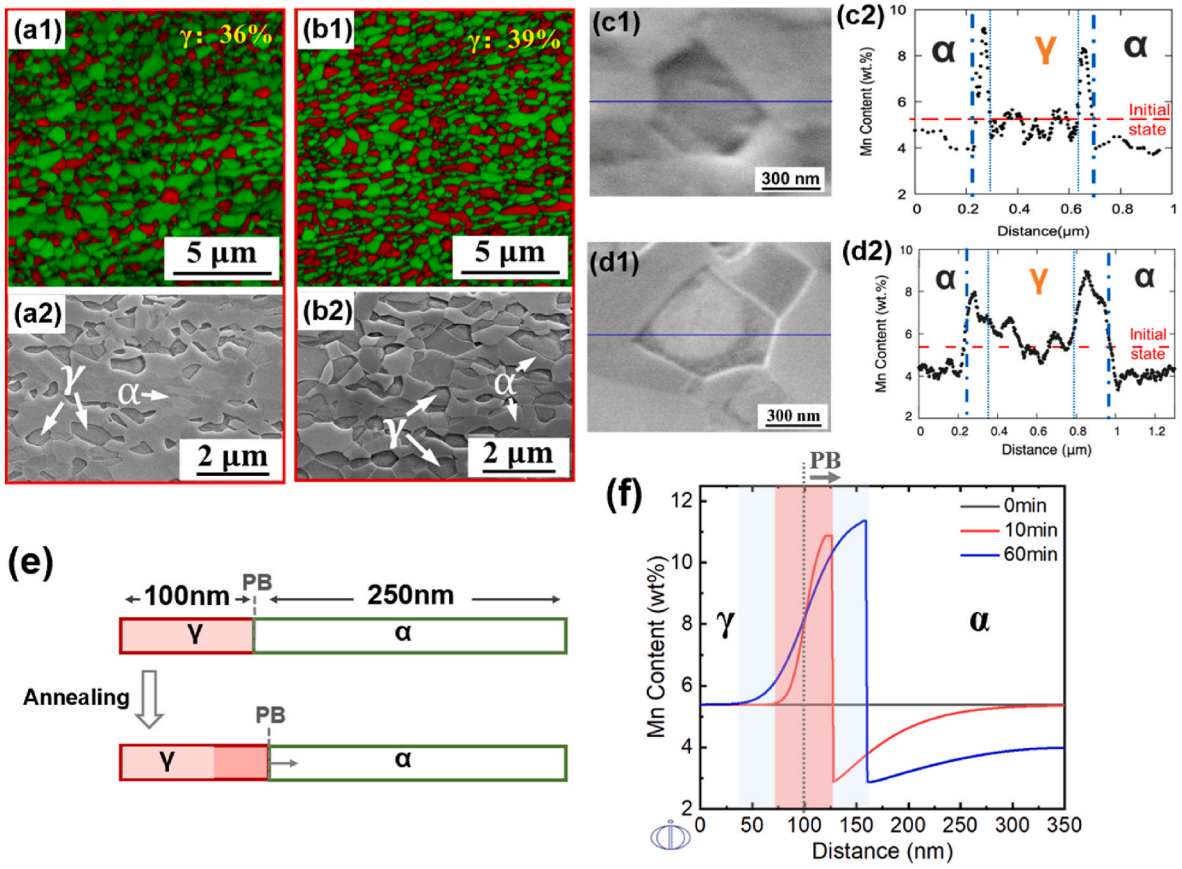

Fig. 1. Microstructure of the (a) FART-10, (b) FART-60 samples: (a1, b1) EBSD phase maps combined with image quality, (a2, b2) SEM micrographs. (c,d) The secondary electron image of austenite and corresponding Mn profile by AES-EBSD in the FART-10 (c) and FART-60 (d) sample. (e) A sketch of the evolution of phase boundary (PB) during annealing. (f) Evolution of Mn profiles after annealing at 660 °C for 0, 10, and 60 min. (γ: austenite; *α*: ferrite).

the mechanical and service properties of MMS.

However, the mechanism of DIMT in RA grains with a chemical core-shell heterogeneity is only qualitatively understood. Several factors, most likely the shell thickness and element enrichment within the shell, are assumed to have a profound influence on the occurrence of the martensitic formation. However, no specific data is available regarding the minimum required composition difference between core and shell, nor the minimum (relative) thickness of the shell necessary to broaden the DIMT range. Additionally, while extensive experimental research exists on the martensitic transformation of metastable austenite under uniaxial tension [23], discussions on the simulation of individual austenite grains during the deformation process remain limited.

In this study, a specific form of chemically heterogeneous austenite, referred to as the compositional core-shell structure, is introduced into MMS. The influence of the compositional core-shell configuration on the stability of austenite and its subsequent mechanical behavior is investigated. Additionally, first ever molecular dynamics (MD) simulations for RA grains with varying compositional combinations and shell thickness are conducted to elucidate the atomistic mechanisms governing the DIMT within core-shell austenite grains.

2. Method

The steel used in this study has the composition of 0.23C–5.38Mn-1.70Al (wt.%). Specimens of 10 × 4× 1 mm^3 were cut from the cold rolled plate and heat treated in a DIL-805ADT type dilatometer. Fig. S1 shows the sketch of Flash-ART. The sample was initially heated to 840 °C (flash temperature) at a rate of 100 °C/s, then rapidly cooled to 660 °C (ART temperature) at 100 °C/s and subsequently annealed for 10 min or 60 min at this temperature [20]. These samples are referred to as FART-10 and FART-60, respectively. The microstructure was characterized using field-emission scanning electron microscopy (FE-SEM) and a PHI-710 type nano-auger electron spectroscopy equipped with electron backscatter diffraction (AES-EBSD). Detailed information can be found in Supplementary Materials.

Dog-bone-shaped tensile specimens had a gauge length, width and thickness of 8 mm, 2 mm and 1 mm, respectively. Tensile tests were performed on an Instron 5565 machine at a strain rate of 10^{-3}/s at room temperature using a non-contact video extensometer. The evolution of RA fraction during tensile testing was recorded by the magnetic induction experiment implemented by an FMP-30 type Feritscope. Ex-situ three-point bending experiments combined with an EBSD analysis were carried out to investigate the mechanical stability of core-shell structured austenite. The kinetics of austenite reversion and the Mn diffusion during isothermal annealing were simulated using DICTRA coupled to the TCFE 7 and MOB 2 databases.

The martensitic transformation of single chemically heterogeneous RA grains during uniaxial straining up to 7.0 % strain was simulated by MD simulations. A spherical FCC (austenite) structure was placed at the center of a BCC (martensite) supercell, and the BCC/FCC interface was designed as an incoherent interface, a design approach that has been validated [24]. The meta-stability of the shell was varied by adjusting the Mn concentration and the thickness. Details of the MD model can be found in the Supplementary Materials.

3. Results and discussion

The microstructures of the FART-10 and FART-60 samples are shown in Fig. 1(a and b). It is obvious that these samples have a typical duplex microstructure consisting of equiaxed RA and granular ferrite. From

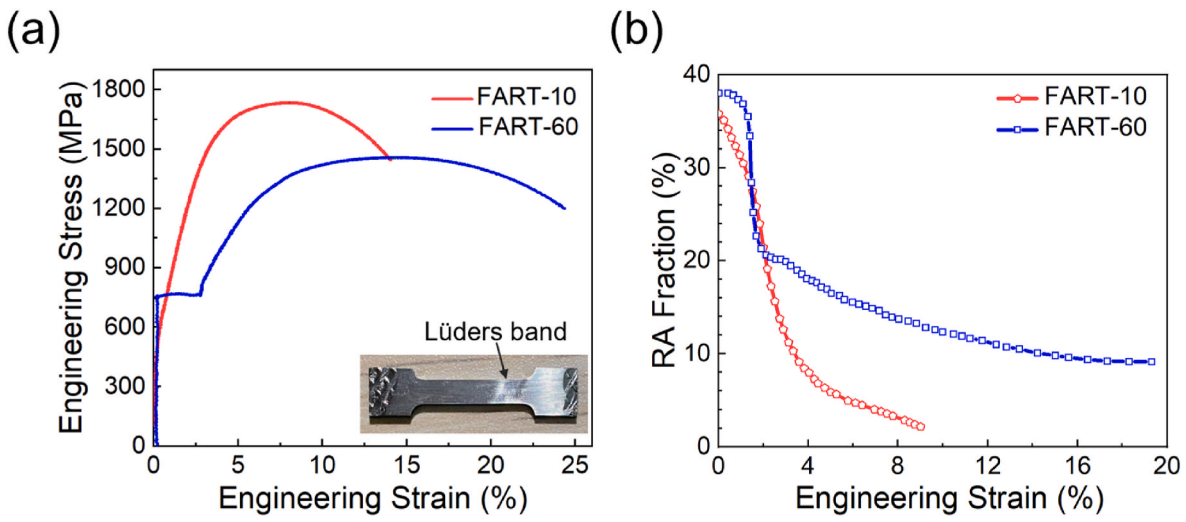

Fig. 2. (A) Engineering stress-strain curves of the FART-10 and FART-60 samples. (b) Corresponding evolution of RA fraction during tensile testing.

SEM images, it is evident that the RA grains have a distinct interior structure with a different response to the electro-polishing process, which is identified as a core-shell structure with a graded distribution of Mn. The volume fraction of RA in the FART-10 sample is slightly lower than that observed in the FART-60 sample, as evidenced by the EBSD phase images. The distribution of Mn in the core-shell austenite was characterized by AES-EBSD in Fig. 1(c and d). It was found that the Mn content in the austenite core is similar to the nominal bulk composition, while the austenite shell, which is marked by blue dashed line, has a higher Mn content. The low Mn core is formed during the flash heating process, while the Mn-rich shell is formed during subsequent ART. It can be clearly seen that the Mn-rich shell of the FART-10 sample is thinner than that of the FART-60 sample. For more information on the detailed formation mechanism of this core-shell austenite, please refer to Ref. [20].

DICTRA simulations were conducted to analyze the formation of the high Mn shell during ART process. During annealing, the phase boundary (PB) of austenite/ferrite migrates towards the ferrite side, which can be derived from the predicted Mn profiles. This indicates that austenite is growing. As illustrated in Fig. 1(e and f), it is predicted that a Mn-rich shell region will emerge. A comparison of the 10 min and 60 min curves revealed that the shell thickness differed by approximately twofold, while the average Mn concentration in the shell remained largely unchanged. This finding is in a qualitative agreement with the microstructure measurements in AES results.

Fig. 2(a) illustrates the stress-strain curves of the FART-10 and FART-60 samples. Fig. 2(b) shows the evolution of RA fraction during deformation. The mechanical properties exhibit contrasting results in these two samples. The ultimate tensile strength decreases with the annealing time increases from 10 min to 60 min. Conversely, the uniform elongation and tensile elongation increased. This is attributed to the different mechanical stability of the austenite in these two samples. The majority of the RA in the FART-10 sample is transformed into martensite, resulting in a higher volume fraction of fresh martensite. This leads to a significant increase in work hardening effect. In contrast, the kinetics of DIMT in the FART-60 sample is slower, resulting in persistent TRIP effects and delayed plastic instability (e.g., necking) [21]. A reduction in the amount of deformation-induced martensite also resulted in a decreased tendency for crack formation and interface decohesion related to fresh martensite [25].

Furthermore, the FART-60 sample exhibits discontinuous yielding behavior as called Lüders band phenomenon, as shown in Fig. 2(a), which is a characteristic feature commonly observed in cold-rolled and annealed MMS [26,27]. However, the Lüders band phenomenon is evidently absent in the FART-10 sample. By comparing the KAM value of the ferrite matrix in Fig. S3, it can be seen that the ferrite of the FART-10 sample has a higher dislocation density due to the shorter annealing time. Concurrently, the austenite of the FART-10 sample is less stable, generating mobile dislocations and work hardening by martensite transformation in the early stage of deformation. An elevated mobile

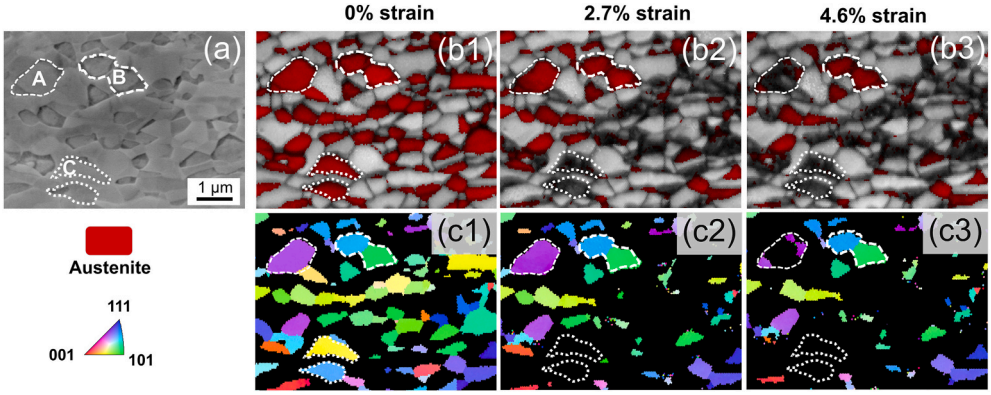

Fig. 3. Mechanical stability of RA grains in the FART-60 sample analyzed by quasi in-situ EBSD measurement. (a) SEM image, (b) Phase-IQ maps and (c) inverse pole figure (IPF) maps of RA showing deformation induced martensite transformation of individual RA grains at different strain level. White dashed line depicts the prior austenite grain boundaries.

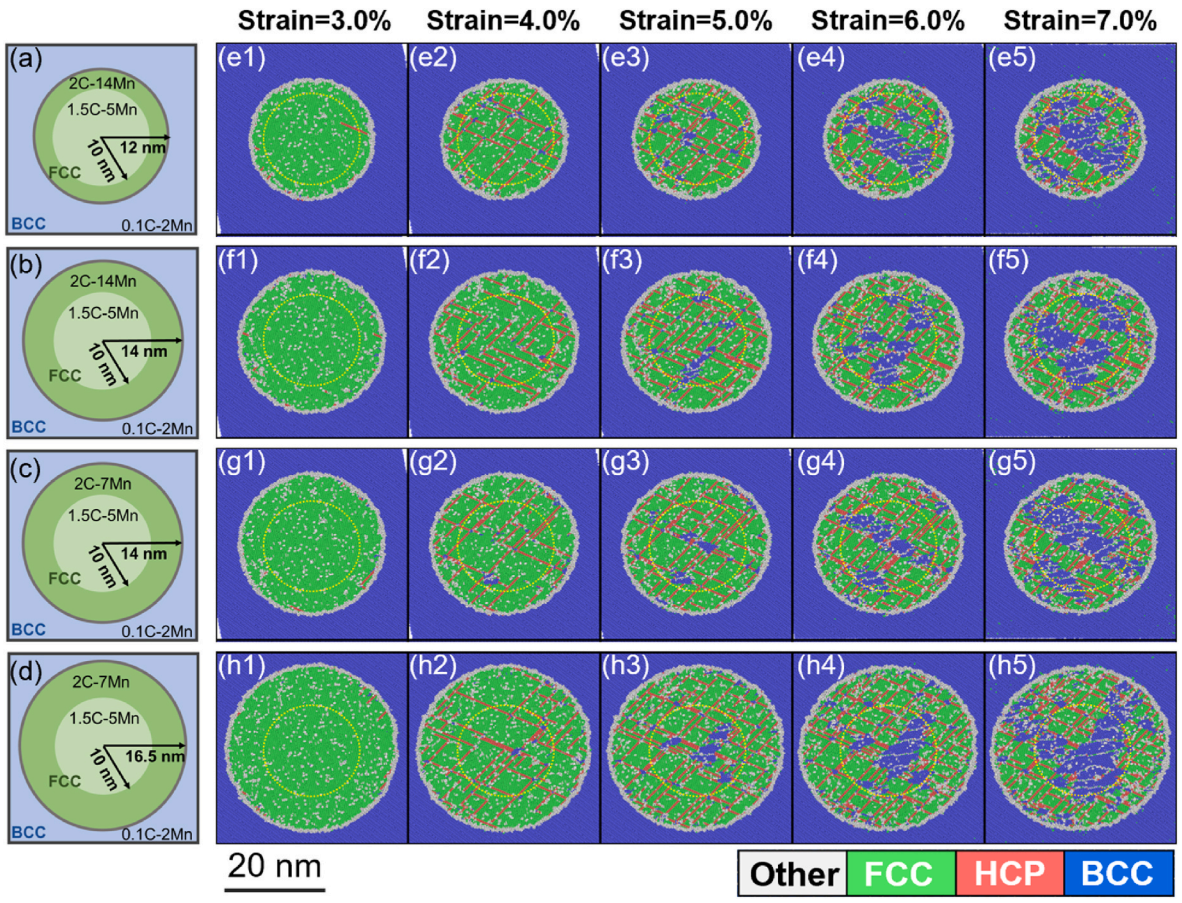

Fig. 4. Sketch of (a)Model-1, (b) Model-2, (c) Model-3 and (d) Model-4. Evolution of the microstructure as a function of the strain for the (e) Model-1, (f) Model-2, (g) Model-3 and (h) Model-4 when viewing the (1 $\bar{1}$ 0) FCC plane. Green marks atoms arranged in a perfect FCC pattern, blue marks the atoms in a perfect BCC pattern, red marks the atoms arranged in HCP stacking fault orientation and grey marks atoms with a crystallographically undefined local surrounding. Yellow dashed line depicts the boundary between core and shell. (For interpretation of the references to colour in this figure legend, the reader is referred to the Web version of this article.)

dislocation density can suppress localized deformation and the formation of Lüders bands [28–30]. Interestingly, the yield strength of Flash-ART specimens significantly decreases as the annealing time is reduced. This observation is primarily attributed to the decreased stability of austenite, resulting in macro-yielding during the elastic stage [5,31].

Fig. 3 illustrates the ex-situ EBSD results obtained in three-point bending experiments of the FART-60 sample. It is noted that the DIMT behavior varied among individual grains. This variation can be categorized into three distinct types, with several representative austenite grains labelled as regions A, B, and C. Classification is based on the extent of martensitic transformation of single austenite grain, which may be complete, partial, or absent under observed strain conditions. In region A, a sequential transformation is observed, with the core area transforming first. Statistical analysis of austenite grains of similar transformation manner discloses that the remaining components invariably exhibit a higher Mn content. The austenite grains in Region B exhibit almost no transformation due to the stabilization effect of the Mn rich austenite shell. As can be observed from the SEM image, the thickness of the shell in this region is notably larger. Furthermore, in region C, there are multiple instances of RA grains without a compositional core-shell structure undergoing a complete transformation to martensite. Earlier studies showed that chemically homogeneous austenite grains typically completely transformed at their specific critical strain level, with only a minority exhibiting gradual stepwise transformation [21–23]. Conversely, the stepwise transformation of metastable RA with chemically heterogeneous structures dominated in this sample. The chemical boundary caused by the heterogeneous distribution of Mn will become the barrier to propagation of the martensite lath during deformation, which is similar to the effect of chemical boundaries observed by Ding [32] during quenching. Such a chemical boundary can stop the growth of martensite by a local reduction in diving force due to the high chemical composition. New martensite formed in the shell will take place in a smaller domain than the complete austenite grain, further extending the strain range over which DIMT occurs. In the case of a single austenite grain with chemical heterogeneity, the integrity of the shell is of paramount importance. If the shell is incomplete, as observed in the grains of region C, it accelerates the progression of the martensitic phase transformation throughout the entire austenite grain. Therefore, the design of the chemical composition inside a single austenite can directly affect the deformation process of martensitic transformation.

DIMT in the core-shell austenite is also investigated by MD modelling. As the comparison to the FART-10 and the FART-60 samples, the thickness of the shell, as well as its Mn concentration are considered as the key shell features. Model-1 and Model-2 are designed featuring identical shell Mn concentrations but different shell thicknesses. Model-3 is designed with a lower Mn% in the shell relative to Model-2, while Model-4 is designed with an increasing thickness of shell as compared to Model-3. The DIMT evolution as a function of the strain and as calculated in the four models is shown in Fig. 4 and Movie. S1. The model is a full 3D model and that the structure evolution is shown for only one FCC plane (the (110) plane going through the very center of the particle). Different impressions are obtained by viewing the structure evolution on

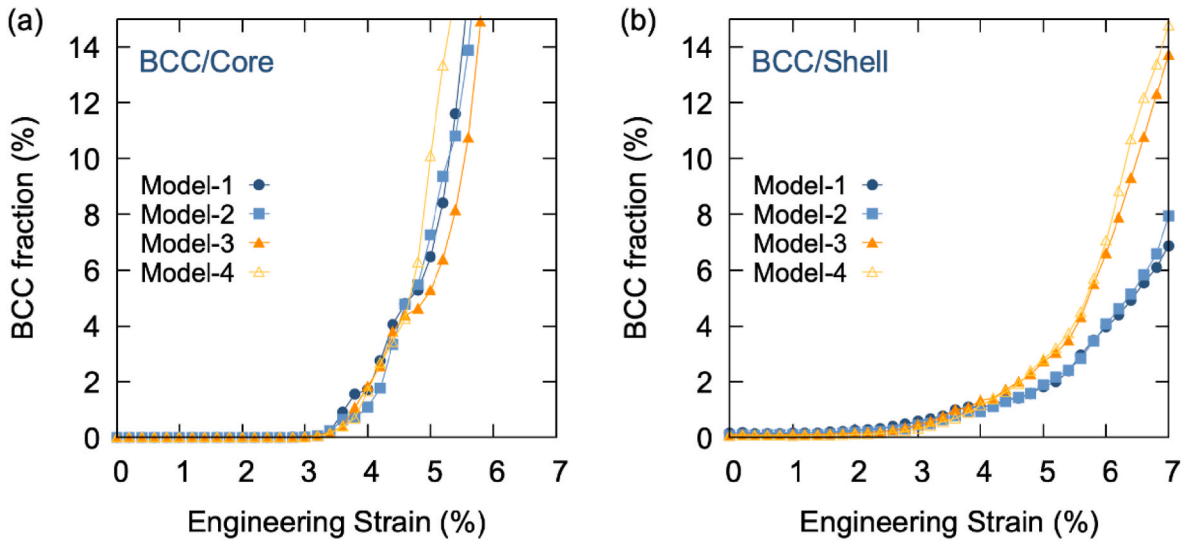

Fig. 5. Fraction of BCC in the core(a) and the shell(b) under different strain loading in four models.

different planes (see Fig. S5). In Fig. 4, up to a strain of 2.5 %, there is nearly no transformation of any sort within the austenitic core for all the four conditions. At a strain of 3.0 %, the formation of HCP stacking faults initiate at the shell-matrix interface, partially propagating into the RA grain. At a strain of 4.0 %, the stacking faults (SFs) form a network as two systems become operational. Interestingly, the stacking faults do not seem to be affected by the presence of the chemical boundaries. Then the first cases of martensite formation become visible. BCC nucleates mainly at the phase interface and the intersection of the SFs. The chemical boundary itself is unlikely to act as a nucleation site for the martensitic transformation. Rather than playing a role in the nucleation of martensite, it primarily controls the propagation of the transformation. With increasing applied strain, the martensite regions grow, in part by absorbing the local stacking faults. The biggest differences between the model predictions become visible when the strain is above 6.0 %. While martensite propagates well into the shell for Model-3 and Model-4, the martensite formation is restricted to the central core as the propagation of the martensite is halted at the chemical boundary for Model-2 (the model with a strong Mn concentration difference and a sizeable shell). The same applies to Model-1 but the effect is less visible due to the thinner shell. Meanwhile, the 3D structure of the martensite formed in Model-2 at 6.0 % strain is shown in the Movie S2. It reveals that the martensite has a blocky structure. Therefore, chemical heterogeneity is unable to impede the formation of martensite nuclei at the interface. However, it does influence the subsequent growth of martensite.

Fig. 5 depicts the BCC evolution averaged over the core and shell of RA particle as a function of the applied strain. Initially, BCC phase formation begins in the austenite shell via the stacking faults. When the strain is less than 4.0 %, the BCC fraction of the core and shell parts of austenite are both in the range of 0~2 %. Chemical heterogeneity indeed has a significant influence on martensite formation. When the strain is increased from 4.0 % to 5.5 %, there is a substantial rise in the volume fraction of BCC in the core, while the BCC volume fraction in the shell undergoes a transformation of less than 5.0 %. In Fig. 5(a), the differences in BCC phase formation within the austenite core among the four models are relatively minor. Conversely, as depicted in Fig. 5(b), the austenite shells in Model-3 and Model-4 exhibit significantly greater instability than those in Model-1 and Model-2, which aligns with the findings presented in Fig. 4. The simulations reveal that the BCC transformation in the core is largely consistent across the various model configurations. Provided that the integrity of the core-shell structure is maintained, the BCC formation in the shell is primarily governed by the local concentration of Mn, rather than the thickness of the shell.

4. Conclusion

In summary, the investigation into the behavior of chemically heterogeneous RA in MMS during the DIMT has been expanded. The manipulation of the core-shell structure produced using the Flash-ART process allows for the modulation of the work hardening behavior of the MMS. Combining experiment and MD simulation, it indicates that the chemical heterogeneity exerts strong barriers to block the propagation of martensitic laths during deformation The higher Mn content in the shell exhibits a stronger core shell effect. Consequently, as a representative example of chemically heterogeneous austenite, the compositional core-shell austenite has demonstrated its considerable potential in modulating the mechanical behavior of MMS.

CRediT authorship contribution statement

Shichun Liu: Writing – review & editing, Writing – original draft, Investigation, Data curation. **Jun Chai:** Writing – review & editing, Validation, Investigation. **Xinhao Wan:** Writing – review & editing, Validation, Investigation, Data curation. **Yan Wang:** Writing – review & editing, Validation, Investigation. **Zhigang Yang:** Supervision, Conceptualization. **Sybrand van der Zwaag:** Writing – review & editing, Conceptualization. **Hao Chen:** Writing – review & editing, Conceptualization.

Originality statement

I write on behalf of myself and all co-authors to confirm that the results reported in the manuscript are original and neither the entire work, nor any of its parts have been previously published. The authors confirm that the article has not been submitted to peer review, nor has been accepted for publishing in another journal. The author(s) confirms that the research in their work is original, and that all the data given in the article are real and authentic. If necessary, the article can be recalled, and errors corrected.

Declaration of competing interest

The authors declare that they have no known competing financial interests or personal relationships that could have appeared to influence the work reported in this paper.

Acknowledgements

Z. G. Yang acknowledges financial support from the National Key R&D program of China (grant No. 2022YFB3705200).

Appendix A. Supplementary data

Supplementary data to this article can be found online at https://doi.org/10.1016/j.msea.2025.147904.

Data availability

Data will be made available on request.

References

[1] R. Ding, Z.B. Dai, M.X. Huang, Z. Yang, C. Zhang, H. Chen, Effect of pre-existed austenite on austenite reversion and mechanical behavior of an Fe-0.2C-8Mn-2Al medium Mn steel, Acta Mater. 147 (2018) 59–69.
[2] Y.K. Lee, J. Han, Current opinion in medium manganese steel, Mater. Sci. Technol. 31 (2015) 843–856.
[3] D.K. Matlock, J.G. Speer, Processing opportunities for new advanced high-strength sheet steels, mater, Manuf. Processes 25 (2010) 7–13.
[4] Z.B. Dai, H. Chen, R. Ding, Q. Lu, C. Zhang, Z. Yang, S. van der Zwaag, Fundamentals and application of solid-state phase transformations for advanced high strength steels containing metastable retained austenite, Mater. Sci. Eng. R 143 (2021) 100590.
[5] Y. Wang, R. Ding, C. Franke, T. Li, X. Rong, P. Wen, Z. Yang, H. Chen, Flash annealing of a chemically heterogeneous medium Mn steel, Scripta Mater. 242 (2024) 115923.
[6] J. Han, S.-J. Lee, J.-G. Jung, Y.-K. Lee, The effects of the initial martensite microstructure on the microstructure and tensile properties of intercritically annealed Fe–9Mn–0.05C steel, Acta Mater. 78 (2014) 369–377.
[7] Z.Y. Liang, Z.H. Cao, J. Lu, M.X. Huang, C.C. Tasan, Influence of co-existing medium Mn and dual phase steel microstructures on ductility and Lüders band formation, Acta Mater. 221 (2021) 117418.
[8] S. Liu, Z. Xiong, H. Guo, C. Shang, R.D.K. Misra, The significance of multi-step partitioning: processing-structure-property relationship in governing high strength-high ductility combination in medium-manganese steels, Acta Mater. 124 (2017) 159–172.
[9] W.C. Jeong, D.K. Matlock, G. Krauss, Effects of tensile-testing temperature on deformation and transformation behavior of retained austenite in a 0.14C-1.2Si-1.5Mn steel with ferrite-bainite-austenite structure, Mater. Sci. Eng., A 165 (1993) 9–18.
[10] C. Song, H. Yu, L. Li, T. Zhou, J. Lu, X. Liu, The stability of retained austenite at different locations during straining of I&Q&P steel, Mater. Sci. Eng. A 670 (2016) 326–334.
[11] J. Park, Y. Hou, J. Min, Z. Hou, H.N. Han, B. He, M.-G. Lee, Understanding plasticity in multiphase quenching & partitioning steels: insights from crystal plasticity with stress state-dependent martensitic transformation, Int. J. Plast. 180 (2024).
[12] R. Blondé, E. Jimenez-Melero, L. Zhao, J.P. Wright, E. Brück, S. van der Zwaag, N. H. van Dijk, Mechanical stability of individual austenite grains in TRIP steel studied by synchrotron X-ray diffraction during tensile loading, Mater. Sci. Eng., A 618 (2014) 280–287.
[13] E. De Moor, D.K. Matlock, J.G. Speer, M.J. Merwin, Austenite stabilization through manganese enrichment, Scripta Mater. 64 (2011) 185–188.
[14] J.T. Benzing, A. Kwiatkowski da Silva, L. Morsdorf, J. Bentley, D. Ponge, A. Dutta, J. Han, J.R. McBride, B. Van Leer, B. Gault, D. Raabe, J.E. Wittig, Multi-scale characterization of austenite reversion and martensite recovery in a cold-rolled medium-Mn steel, Acta Mater. 166 (2019) 512–530.
[15] X.G. Zhang, G. Miyamoto, Y. Toji, Y. Zhang, T. Furuhara, Role of cementite and retained austenite on austenite reversion from martensite and bainite in Fe-2Mn-1.5Si-0.3C alloy, Acta Mater. 209 (2021) 116772.
[16] R. Ding, C.F. Zhang, Y. Wang, C.X. Liu, Y. Yao, J. Zhang, Z. Yang, C. Zhang, Y. Liu, H. Chen, Mechanistic role of Mn heterogeneity in austenite decomposition and stabilization in a commercial quenching and partitioning steel, Acta Mater. 250 (2023) 118869.
[17] B.H. Sun, W.J. Lu, B. Gault, R. Ding, S.K. Makineni, D. Wan, C.H. Wu, H. Chen, D. Ponge, D. Raabe, Chemical heterogeneity enhances hydrogen resistance in high-strength steels, Nat. Mater. 20 (2021) 1629–1634.
[18] G. Gu, J.H. Kim, H.H. Lee, A. Zargaran, M. Koo, S.H. Kim, J.S. Lee, D.-W. Suh, Room temperature quenching and partitioning (RT-Q&P) processed steel with chemically heterogeneous initial microstructure, Mater. Sci. Eng. A 851 (2022) 143651.
[19] J.H. Kim, G. Gu, M.-H. Kwon, M. Koo, E.-Y. Kim, J.-K. Kim, J.S. Lee, D.-W. Suh, Microstructure and tensile properties of chemically heterogeneous steel consisting of martensite and austenite, Acta Mater. 223 (2022) 117506.
[20] X.H. Wan, G. Liu, R. Ding, N. Nakada, Y.-W. Chai, Z. Yang, C. Zhang, H. Chen, Stabilizing austenite via a core-shell structure in the medium Mn steels, Scripta Mater. 166 (2019) 68–72.
[21] B.H. Sun, R. Ding, N. Brodusch, H. Chen, B. Guo, F. Fazeli, D. Ponge, R. Gauvin, S. Yue, Improving the ductility of ultrahigh-strength medium Mn steels via introducing pre-existed austenite acting as a “reservoir” for Mn atoms, Mater. Sci. Eng. A 749 (2019) 235–240.
[22] J. Zhang, B.H. Sun, Z.G. Yang, C. Zhang, H. Chen, Enhancing the hydrogen embrittlement resistance of medium Mn steels by designing metastable austenite with a compositional core–shell structure, Acta Metall. Sin. 36 (2023) 1059–1077.
[23] Y. Zou, Q. Gao, H. Ding, Y. Zhang, Z. Tang, Investigations on austenite stability and martensitic transformation kinetics of a medium Mn steel under different strain states, Int. J. Plast. 171 (2023).
[24] J. Chai, H. Dong, J.-Y. Zhang, K. Shen, Z. Yang, H. Chen, On the role of interfacial coherency and carbon in niobium segregation at ferrite/austenite interface: an atomistic study, Scripta Mater. 247 (2024) 116109.
[25] Q. Lai, O. Bouaziz, M. Gouné, L. Brassart, M. Verdier, G. Parry, A. Perlade, Y. Bréchet, T. Pardoen, Damage and fracture of dual-phase steels: influence of martensite volume fraction, Mater. Sci. Eng., A 646 (2015) 322–331.
[26] B. Sun, N. Vanderesse, F. Fazeli, C. Scott, J. Chen, P. Bocher, M. Jahazi, S. Yue, Discontinuous strain-induced martensite transformation related to the Portevin-Le Chatelier effect in a medium manganese steel, Scripta Mater. 133 (2017) 9–13.
[27] X.G. Wang, L. Wang, M.X. Huang, Kinematic and thermal characteristics of Lüders and Portevin-Le Châtelier bands in a medium Mn transformation-induced plasticity steel, Acta Mater. 124 (2017) 17–29.
[28] Q.H. Han, Y.L. Zhang, L. Wang, Effect of annealing time on microstructural evolution and deformation characteristics in 10Mn1.5Al TRIP steel, Metall. Mater. Trans. A 46a (2015) 1917–1926.
[29] B.H. Sun, Y. Ma, N. Vanderesse, R.S. Varanasi, W. Song, P. Bocher, D. Ponge, D. Raabe, Macroscopic to nanoscopic in situ investigation on yielding mechanisms in ultrafine grained medium Mn steels: role of the austenite-ferrite interface, Acta Mater. 178 (2019) 10–25.
[30] J.W. Ma, Q. Lu, L. Sun, Y. Shen, Two-step intercritical annealing to eliminate Lüders band in a strong and ductile medium Mn steel, Metall. Mater. Trans. A 49 (2018) 4404–4408.
[31] B. Mirshekari, A. Zarei-Hanzaki, A. Barabi, A. Moshiri, H.R. Abedi, S.J. Lee, H. Fujii, Optimizing the austenite stability in a ferritic lightweight steel through thermomechanical processing, Mater. Char. (2020) 110367.
[32] R. Ding, Y.J. Yao, B.H. Sun, G. Liu, J.G. He, T. Li, X.H. Wan, Z.B. Dai, D. Ponge, D. Raabe, C. Zhang, A. Godfrey, G. Miyamoto, T. Furuhara, Z.G. Yang, S. van der Zwaag, H. Chen, Chemical boundary engineering: a new route toward lean, ultrastrong yet ductile steels, Sci. Adv. 6 (2020) eaay1430.